Article

Simultaneous Voltammetric Determination of Acetaminophen and Isoniazid (Hepatotoxicity-related Drugs) utilizing Bismuth Oxide Nanorod Modified Screen-printed Electrochemical Sensing Platforms

Bahaa G. Mahmoud, Mohamed Khairy, Farouk A Rashwan, and Craig E Banks

Anal. Chem., **Just Accepted Manuscript** • DOI: 10.1021/acs.analchem.6b05130 • Publication Date (Web): 06 Jan 2017

Simultaneous Voltammetric Determination of Acetaminophen and Isoniazid (Hepatotoxicity-related Drugs) utilizing Bismuth Oxide Nanorod Modified Screen-printed Electrochemical Sensing Platforms

Bahaa G. Mahmoud,[†] Mohamed Khairy,[†]* Farouk A. Rashwan[†] and Craig E. Banks [‡]*

† Chemistry Department, Faculty of Science, Sohag University, 82524.

‡ Faculty of Science and Engineering, Manchester Metropolitan University, Chester Street, Manchester M1 5GD, UK.

ABSTRACT: To overcome the recent outbreaks of hepatotoxicity related-drugs, a new analytical tool for the continuously determination of these drugs in human fluids is required. Electrochemical based analytical methods offer an effective, rapid and simple tool for on-site determination of various organic and inorganic species. However, the design of a sensitive, selective, stable and reproducible sensor is still a major challenge. In the present manuscript, a facile, one-pot hydrothermal synthesis of bismuth oxide ($Bi_2O_{2.33}$) nanostructures (nanorods) was developed. These BiO nanorods were cast onto mass disposable graphite screen-printed electrodes (BiO-SPEs) allowing the ultrasensitive determination of acetaminophen (APAP) in the presence of it's the common interference isoniazid (INH) which are both found in drug samples. The simultaneous electroanalytical sensing using BiO-SPEs exhibited strong electrocatalytic activity towards the sensing of APAP and INH with an enhanced analytical signal (voltammetric peak) over that achievable at unmodified (bare) SPEs. The electroanalytical sensing of APAP and INH are possible with accessible linear ranges from 0.5 to 1250 μM and 5 to 1760 μM with limits of detection (3σ) of 30 nM and 1.85 μM, respectively. The stability, reproducibility and repeatability of BiO-SPE were also investigated. The BiO-SPEs were evaluated towards the sensing of APAP and INH in human serum, urine, saliva and tablet samples. The results presented in this paper demonstrate that BiO–SPEs sensing platforms provide a potential candidate for the accurate determination of APAP and INH within human fluids and pharmaceutical formulations.

Hepatotoxicity implies chemical-driven liver damage and the liver acts as central organ for metabolism of virtually every foreign substance (*i.e.* drugs).[1] More than 900 drugs and herbs have been reported to cause severe liver disease and drugs account for 20–40% of all instances of fulminant hepatic failure. Approximately 75% of the idiosyncratic drug reactions result in liver transplantation or death.[2] Drug-induced liver disease is responsible for 5% of all hospital admissions and 50% of all acute liver failures in western countries.[3] Therefore, physicians must be vigilant in identifying drug-related hepatic injury because early detection can reduce the severity of induced hepatotoxicity. Knowledge of the commonly implicated drugs is essential in clinical diagnosis. In the United States, approximately 2000 cases of acute liver failure occur annually and nearly 60% of these are caused by acetaminophen or idiosyncratic drug reactions.[4] Development of an analytical tool for accurate determination of acetaminophen (APAP) and its interferences has a significant importance not only in clinical diagnosis but also for quantity control of their pharmaceutical formulations.

Acetaminophen, APAP (N-acetyl-p-aminophenol) is known as Paracetamol or Tylenol and is one of the most widely antipyretic and analgesic drugs these days. It is an extremely weak acid (pKa = 9.7) and is, therefore, essentially unionized at physiological pH values. It is commonly used as a safe and effective painkiller associated with headache, backache, arthritis and postoperative pain. It has been also used for reduction of cough, cold and fevers symptoms.[5] The analgesic–antipyretic effect of APAP is similar to aspirin, but APAP is normally preferred especially for the patients who are sensitive to acetylsalicylic acid.[6] The mechanism of action of APAP to relieve pain is linked to inhibition of prostaglandin synthesis in the central nervous system and relieves fever by sedating hypothalamic heat-regulating centre.[7] Single doses of APAP shows analgesic activity in a variety of acute pain syndromes without any side effects; however, overdoses (4.0 g/daily) are now the most common cause of acute liver failure, which may progress to death. Therapeutic concentration levels in plasma is between 10-25 μg/mL, however, its toxicity concentration level is higher than 200 μg/mL (≈ 1.33mM). It is therefore important to develop an analytical technique to determine acetaminophen in pharmaceutical dosages and human fluids accurately. A variety of analytical methods such as titrimetry,[8] UV/Vis spectrophotometry,[9] flow-injection,[10] high performance liquid chromatography (HPLC),[11] chemiluminescence,[12] capillary electrophoresis (CE),[13] and electrochemical techniques[14-16] have been recently reported. While, improving the analytical method in terms of sensitivity, stability, repeatability and selectivity are essential for human health and security.[17]

Isoniazid (isonicotinoyl hydrazine, INH) is an antibacterial drug available as more than 300 mg tablets for oral administration. It is one of effective tuberculostatic drugs widely used for prevention and treatment of tuberculosis due to restriction of mycobacterium strains[18,19] and is an essential and indispensable basic remedy for tuberculosis. However, it is associated with hepatotoxicity and peripheral neuropathy while slow acetylators may be at increased risk of toxicity. The toxicity can occur with the acute ingestion of as little as 1.5 g (10.9 mM). Moreover, hydrazine was produced during the isoniazid metabolism not only inducing hepatotoxicity with inflammation but also might lead to death.[20] The Public Health Service Surveillance Study examined 13,838 patients treated with INH in USA; there were eight deaths among 174 cases of hepatitis. Furthermore, some antipyretic drugs like APAP should be combined with INH to control fever during the course of disease. This combination enhances drug-drug interactions, ultimately affecting their bioavailability and pharmacokinetic behaviors. Such interaction might also increase the extent of bioactive drug resulting in its toxic effects or decrease it to sub-therapeutic levels in blood that may lead to antimicrobial resistance. The pre-treatment with INH could increase the APAP-induced hepatic necrosis score by 85%.[21] Therefore, the people taking INH and APAP are at risk of APAP- toxicity.[22] The patients treated with INH should be carefully monitored and interviewed periodically every month intervals. HPLC,[23] spectrophotometry,[24] chemiluminescence,[25] CE,[26] and electrochemical technique[27,28] have been reported recently for determination of INH. Although electrochemical methods offer fast response, easy handling and low operating cost, there is only one literature report detailing the simultaneous determination of APAP and INH using thionine immobilized multi-walled carbon nanotube modified carbon paste electrode.[29] However, the cost effective, portability and difficulty to use such electrodes leads us to explore new generation of screen-printed electrodes in a form of a point-of-care sensor.

Herein, we explored the simultaneous voltammetric determination of APAP and its common interference of INH using BiO nanostructured modified screen-printed electrodes (SPEs). One-pot hydrothermal synthesis of BiO nanostructures has been developed for the first time. The dispersed BiO nanorods are simply drop-casted onto SPE surfaces after which the sensors are ready to be utilized. The BiO-SPEs are found to exhibit greater electrocatalytic activity, stability, and reproducibility for the simultaneous determination of APAP and INH in aqueous pH 2 buffer solution over unmodified (bare) SPEs. The suggested BiO-SPE electrochemical sensing platform was successfully employed to detect the concentration of APAP and INH in human fluids and pharmaceutical formulations.

EXPERIMENTAL SECTION

All chemicals were used without any further purification. Bismuth nitrate ($Bi(NO_3)_3$, 99.9%) was obtained from Sigma-Aldrich Company Ltd. Acetaminophen was kindly supplied by Glopal Napi Pharmaceutical Co. (6th of October, Egypt) and Isoniazid purchased from BDH Co., Ltd. All experiments were performed in Britton Robinson (BR) buffer solutions containing 0.05 M of each boric acid, phosphoric acid and acetic acid and 0.1 M sodium hydroxide was added to reach the required pH value of the solution.

Synthesis of bismuth oxide nanostructures: The hydrothermal synthesis of bismuth oxide nanorods has been developed using bismuth nitrate $Bi(NO_3)_3$ and ammonium hydroxide (NH_4OH, 28%) as starting precursors without using any further additives or template-directing agents. In our synthesis approach, 2.42 g of $Bi(NO_3)_3$ was dissolved in 50.0 mL acidified deionized water. The transparent solution of $Bi(NO_3)_3$ was introduced into a 100.0 mL Teflon-lined stainless steel autoclave. Then, NH_4OH solution was introduced until a white precipitate was formed. The solution mixture has a pH value of 2.2. The autoclave was sealed and placed in an oven at 160 °C for 12 hours for hydrothermal treatment after which was then allowed to cool at room temperature. After the hydrothermal process, a white precipitate was collected and rinsed several times with ethanol/water mixture to remove the remaining agents before being dried at 50 ^{o}C. Finally, the large yield of bismuth oxide nanorods was formed by calcination at 300 °C for 3 hours.

Fabrication of bismuth oxide modified screen-printed electrode: The SPEs were fabricated in-house with appropriate stencil using a DEK 248 screen-printing machine (DEK, Weymouth, U.K.).These electrodes have been used extensively in previous studies For their fabrication, first, a carbon-graphite ink formulation (product code C2000802P2; Gwent Electronic Materials Ltd., U.K.) was screen-printed onto a polyester (Autostat, 250 μm thickness) flexible film (denoted throughout as standard-SPEs); these electrodes have been used extensively in other work.[17, 30-37] This layer was cured in a fan oven at 60 °C for 30 minutes. Next, a silver/silver chloride reference electrode was included by screen-printing Ag/AgCl paste (product code C2040308D2; Gwent Electronic Materials Ltd., U.K.) onto the polyester substrates and a second curing step was undertaken where the electrodes were cured at 60 °C for 30 minutes. Finally, a dielectric paste (product code D2070423D5; Gwent Electronic Materials Ltd., U.K.) was then printed onto the polyester substrate to cover the connections. After a final curing at 60 °C for 30 minutes these SPEs are ready to be used. These SPEs have been reported previously and shown to exhibit a heterogeneous electron transfer (HET) rate constant, k^o, of *ca.* 10^{-3} cm s^{-1}, as measured using the $[Ru(NH_3)_6]^{3+/2+}$ redox probe.

The SPEs were modified with BiO nanostructures by a simple drop-casting process. The BiO suspension was prepared by dispersing 5.0 mg of BiO powder in 5.0 mL deionized water and then sonicated for 10 min. 5.0 μL of the BiO suspension was dropped onto the SPE surface and left it to dry in oven at 50 ^{o}C for 30 minutes.

Real sample analysis: Fresh human blood (5 mL) was collected from healthy volunteers in the hospital of Sohag University, with the aliquot of the sample collected in a test tube. The collected blood sample was kept at room temperature for 30 minutes and then centrifuged for 5 minutes at 3500

rpm. Finally, the supernatant serum sample was collected in a new test tube and stored at 4 ^{o}C in a refrigerator when not in use. The APAP and INH in low, medium and high concentration levels have been spiked into blood serum sample. Then, the recovery test was carried out by spiking of APAP and INH in serum sample into10 mL electrochemical cell containing pH 2.0 B.R buffer and differential pulse voltammetry (DPV) was recorded. A standard addition method was used to determine the APAP and INH concentrations.

The applicability of BiO-SPEs was also tested in several real samples (human blood, urine, saliva and pharmaceutical tablets). APAP and INH were injected to the real samples and left for 1.0 h, stored at 4 ^{o}C in a refrigerator. For human blood, the sample was centrifuged for 5 minutes at 3500 rpm. The supernatant serum sample containing APAP and INH was collected in a new test tube and the pH was adjusted to pH 2 using hydrochloric acid. Then, A 100 µL of serum samples was dropped onto three electrode configuration cell of BiO-SPEs working electrode. DPV was utilised and the standard addition method was used to determine the APAP and INH concentration.

For urine and saliva samples, 300 µL of saliva or urine samples was also injected with APAP and INH and stored at 4 ^{o}C in refrigerator for 1.0 h. Then, the sample solution was adjust to pH 2 using HCl. A 100 µL of adjusted saliva or urine samples was dropped onto the working electrode of the BiO-SPEs and DPV was utilised.

Ten tablets of APAP (Paracetamol, 500 mg) and INH (Isocid forte, 200 mg) pharmaceutical formulations were accurately weighed and finely grinded in a mortar. A chosen amount of these powders were transferred into a 100 mL volumetric flask. About 20 mL of ethanol was added, swirled and sonicated for 5 min. The volume of the sample was completed to the mark and finally filtered using fine filter paper. The first portion of the filtrate was rejected. A specific volume of the stock solution of the drugs was diluted with deionized water to obtain the suitable concentration. A 100 µL of a particular concentration of APAP and INH solutions were diluted by B.R. buffer pH 2 and dropped onto the BiO-SPEs and compared with the standard concentrations of APAP and INH drugs. The concentrations of APAP and INH were measured by DPV method.

Characterization of bismuth oxide nanostructures: The morphology of the bismuth oxide sample was investigated using field emission scanning electron microscopy (FE-SEM, JEOL model 6500). The bismuth oxide powder was ground and fixed onto a specimen stub using double-sided carbon tape. To obtain high-resolution micrographs, a 10 nm Pt film was coated on the bismuth oxide using anion sputtering (Hitachi E-1030) at room temperature. The SEM was operated at 15 KeV to obtain high-resolution SEM images. Further, Transmission electron microscopy (TEM) of BiO sample was performed using a JEOL JEM microscope model 2100. TEM was conducted at an acceleration voltage of 200 kV to obtain a lattice resolution of 0.1 nm. TEM images were recorded using a CCD camera. The BiO sample was dispersed in ethanol solution by using an ultrasonic bath, and then dropped on a copper grid. Prior to inserting the samples into the TEM column, the grid was vacuum dried for 20 min.

Wide-angle powder X-ray diffraction (XRD) was performed by X-ray diffractometer (Model FW 1700 series, Philips, Netherlands) using with monochromatic CuK_{α} radiation (λ = 1.54 Å), employing a scanning rate of 0.06°/min and 2θ ranges from 20° to 80°. The diffraction data were analysed using PDF software Released in1996.

The textural surface properties and pore size distribution was determined by N_2 adsorption/desorption isotherms at 77 K with a BELSORP36 analyzer (JP. BEL Co., Ltd.). The specific surface area (S_{BET}) was calculated using the Brunauer–Emmett–Teller (BET) method with multipoint adsorption data from the linear segment of the N_2 adsorption isotherm. The pore size distribution was determined from the analysis of desorption branch of isotherm using Barrett-Joyner-Halenda (BJH) method.

The voltammetric measurements were carried out using Autolab 302N potentiostat/galvanostat workstation and data was controlled by NOVA software version 1.11.2 for Windows7. Experiments were performed using 3 mm bismuth oxide modified graphite screen-printed working electrode, platinum counter electrode and saturated calomel electrode (SCE) reference electrode.

RESULTS AND DISCUSSION

Physicochemical characterization of the bismuth oxide nanostructures: Bismuth oxide is an important metal oxide semiconductor which has been intensively investigated due to excellent optical and electrical properties such as wide band-gap, high refractive index, high dielectric permittivity and good photoconductivity.[38,39] Owing to these unique features, it has been widely used in many applications such as schottky barrier solar cells, sensor technology, varistors, optical coatings, photovoltaic cells, microwave integrated circuits and transparent ceramic glass manufacturing.[38,39] Control over the morphology, size, crystallinity and surface composition of bismuth oxide nanostructures can be effectively alter its physicochemical characteristics. Herein, a simple, one-pot hydrothermal synthesis of BiO nanostructures has been carried out by adjusting the pH of acidic solution of bismuth nitrate by ammonium hydroxide solution until a white precipitate was formed. After which, calcination of obtained white powder at 300 ^{o}C for 3.0 hours was performed.

Although the particle morphology, composition and size are crucial factors for metal oxide nanostructures applicability,[30, 30-42] very few literatures have been reported to control the size and morphology of bismuth oxide (Bi_2O_3) nanostrucures.[38, 39, 43] Figure 1A shows the SEM micrograph of bismuth oxide sample synthesized by a facile one-pot hydrothermal method without any additives. The SEM image exhibits highly dispersed and nano-sized bismuth oxide with rod-

like morphology. The average diameter of bismuth oxide nanorods is about 50 nm with a length of 400 nm. Further, TEM image (Figure 1B) shows dispersed BiO nanorods with an average diameter of 50 nm and a length of about 300-400 nm. Significantly, our synthesis conditions provide a facile and template-free method for fabrication of highly crystalline bismuth-rich bismuth oxide nanostructures without any agglomeration.

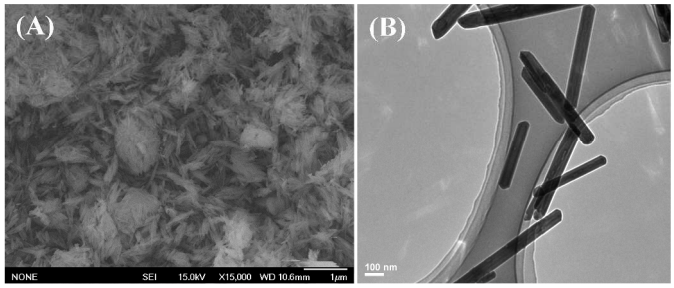

Figure 1 (A) FE-SEM and (B) TEM images of BiO nanostructures prepared via a simple hydrothermal treatment.

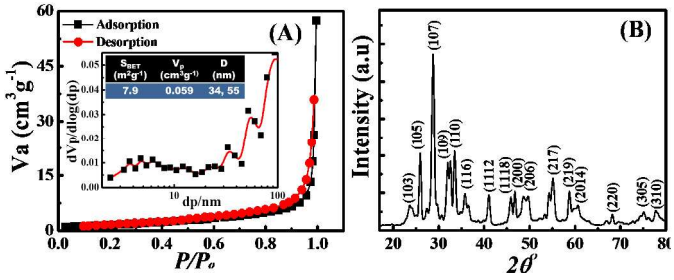

Figure 2 (A) Nitrogen adsorption /desorption isotherm and its corresponding BJH pore distribution curve, (B) Typical X-ray powder diffraction pattern of the BiO nanostructures

The specific surface area and porosity of the BiO nanorods were investigated by using N_2 adsorption/desorption isotherms. Figure 2, shows a representative N_2 adsorption/desorption isotherm measured at 77 K and distribution of pore diameter for the synthesized BiO sample. The N_2 isotherm can be categorized as type IV with a distinct H3 hysteresis loop was observed in the range of 0.5–1.0 P/P_0, which was characteristic of macro-/ meso-porous materials. The S_{BET} specific surface area was calculated to be 7.9 $m^2 g^{-1}$. Further, the BiO nanorods contained small mesopores with average diameter about 5, 34 and 55 nm, determined by using the Barret–Joyner–Halenda (BJH) method (Figure 2B). The formation of the lower pore size was probably related to the pores present inside the nanorods, which were formed between primary crystallites. In turn, the higher pore size may be related to the voids between the nanorod particles. Such bimodal porous texture of BiO nanorods is very important in electrochemical sensors because it provides enhanced surface area with macro-/ mesopores. These significant features are the key factors for controlling the diffusion pathway of analytes and alter the solution/electrode interface. Furthermore, the crystal structure of the bismuth oxide powder was characterized using XRD and is shown in Figure 2(B). Different diffraction peaks have been indexed with corresponding (hkl) values using JCPDS data file (27-0051) indicating the nano-crystalline structure of the bismuth oxide. The XRD patterns also confirmed preferential growth of tetragonal phases of $Bi_2O_{2.33}$. Interestingly, the XRD shows stoichiometric changes due to oxygen loss. The slight excess of Bi atoms over oxygen atoms in the tetragonal crystal might offer enhanced electron conductivity for better electrochemical performance.

Electrochemical characterization of bismuth oxide nanostructures: To explore the electrochemical performance of (BiO-SPE), the redox probe of $K_3Fe(CN)_6$ has been studied. Figure 3 and Figure S1 show the cyclic voltammetric curves of BiO modified and bare/unmodified screen printed-electrode in 2×10^{-4} mol.L^{-1} $K_3[Fe(CN)_6]$ / 0.1 mol.L^{-1} KCl recorded over a range of voltammetric scan rates. In both cases, the peak heights were increased with increasing the potential scan rate as well as they are linearly correlated with the square root of the scan rates in the range of 10–200 mV/s (as shown in Figure 3B) suggesting a diffusion controlled process of reactants at the electrode surface. Comparing the CV curves at 10 mV/s, it was found that the peak current ratio (I_{pc}/I_{pa}) is equal to 1.1 for the unmodified SPEs while the BiO-SPEs exhibit a I_{pc}/I_{pa} equal to 1.37. Therefore, the BiO-SPEs may be claimed to promote electron transfer reaction better than the unmodified SPE does. Moreover, the peak separation was slightly increased to 179 mV at the BiO-SPEs compared to 170 mV for unmodified SPEs, which is due to the electrostatic repulsion between $[Fe(CN)_6]^{3-}$ and BiO nanorod surface. This behaviour suggests that the BiO surface is more negatively charged, in agreement with the behaviour observed for Titanate nanotubes.[40] The result show in Figure 3 that the BiO nanorods have enhanced the electrochemical signal / performance of the graphite screen-printed electrode by an order of ~2 times, which might be attributed to the free bismuth atoms on the surface of BiO nanoparticles that facilitated the electron transfer process and/or an increase in the electrochemical surface area (*i.e.* the BiO kinetics dominate).[30]

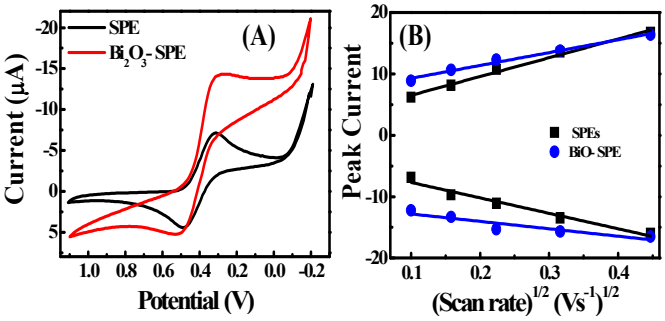

Figure 3 (A) Cyclic voltammetric curves of SPE and BiO-SPEs in 0.1 M KCl containing 2×10^{-4} M Potassium ferricyanide. (B) Cyclic voltammetric peak current analysis at various scan rates.

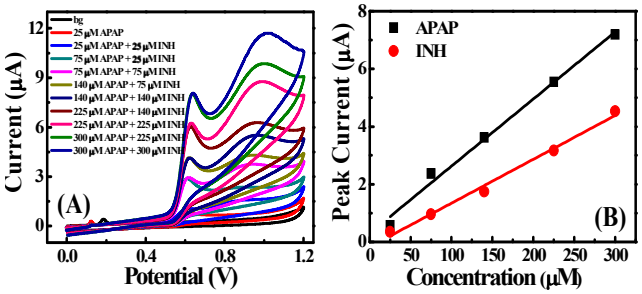

Figure 4 (A) Cyclic voltammetric curves observed at BiO nano-rods modified SPEs for successive additions of APAP and INH into B.R. buffer pH 2, (B) Corresponding cyclic voltammetric peak current analysis of APAP and INH additions at scan rate 50 mVs^{-1}.

Electrochemical behaviour of APAP and INH: The voltammetric behaviour of APAP and INH were investigated on BiO-SPEs because the isoniazid was considered as an important drug interferes with APAP in pharmaceuticals. Figure S2 illustrates the cyclic voltammograms of 75 $\mu mol.L^{-1}$ APAP and 75 $\mu mol.L^{-1}$ INH obtained in B.R. Buffer solution (pH 2.0) on unmodified and BiO modified SPEs. BiO nanorods showed an efficient electrocatalytic activity for the oxidation of APAP and INH molecules compared to bare SPEs. In order to explore the efficiency of BiO nanorods, different metal oxide nanostructure materials and bismuth-based materials have been synthesised and used for determination of APAP and INH drugs. NiO,[40] CuO,[30] CdO,[44] MgO,[45] , Bi_2S_3,[46] $Bi_{12}NiO_{19}$[47] and bulky Bi_2O_3 have been investigated (as shown in Figure S3). Interestingly, BiO nanorods-SPEs show high sensitivity and stability as well as good peak potential separation in the determination of APAP and INH molecules. Figure 4A shows cyclic voltammetry of successive additions individually of APAP and INH in BR buffer pH 2.0 at scan rate of 50 mVs^{-1} on BiO-SPEs. As it can be seen, APAP and INH exhibit well-defined oxidation peaks around 0.64 and 1.02V, respectively. The peak potentials difference of about 0.38 V (vs. SCE) between both oxidation peaks clearly allows the simultaneous determination of APAP and INH without any interference. Of interest is the voltammetric peak current response of APAP and INH on the BiO-SPE linearly correlates with their concentrations up to 300 $\mu mol.L^{-1}$ as shown in Figure 4B.

Next attention was turned to explore the effect of pH upon the electrochemical signals of APAP and INH, since the selection of suitable medium is very important for simultaneous electrochemical responses of APAP and INH. Figure S4 shows the cyclic voltammetric curves of 100µM of APAP and 100µM INH onto BiO-SPEs in different pH values in different pH values. Moreover, effect of solution pHs on the CV curves for 50 $\mu mol.L^{-1}$ APAP and 50 $\mu mol.L^{-1}$ INH onto BiO-SPEs also presented. With increasing the pH value, the oxidation potentials of APAP and INH were shifted to less positive potential values and the oxidation peak of INH interferes with oxidation peak of APAP. This result indicates that, the pH 2 is the suitable medium for simultaneous determination of APAP and INH. A plot of peak potential (E) vs. pH, as shown in Figure S4D, was constructed where a linear range with gradient of 43 mV/pH and 64 mV/pH for APAP and INH, respectively were observed (For *APAP; E/V = 0.043 Ep (V) /pH + 0.55 V, R^2= 0.95; For INH; E/V = 0.064 Ep (V) /pH + 0.83 V, R^2= 0.98*). These values are close to that of Nernstian slope (59 mV/pH) which related to transfer an equal number of protons and electrons and likely to be in agreement with the literature.[5,29,50-59] Therefore, we supposed that the oxidation of APAP and INH at BiO–SPEs is likely involves $2e^-/2H^+$ transfer processes as shown in Scheme 1. In APAP, it was observed that, the peak current of APAP was decreased in alkaline solutions. The pK_a value APAP in solution is about 9.7, above this value the APAP was existed in deprotonated form which exhibit a net negative charge. Such negative charge will be repulsed with the negative charge of the BiO-SPE surface. Moreover, the deprotonated APAP form is likely to be more soluble in aqueous solution than its neutral species; hence the amount of diffused APAP to BiO-SPEs surface is much lower than its fraction in the solution. Therefore, the acidic medium is highly desirable for oxidation of APAP on BiO-SPEs. The oxidation of APAP includes transfer of $2e^-/2H^+$ to form quinone-like structure followed by hydrolysis of the acetamide functional group to produce *p*-aminophenol (Scheme 1). Further, the pK_a value of INH is about 4.84 and therefore, protonated form of isoniazid will be also very important in the electrostatic attraction with negatively charged BiO nanorods. In alkaline medium, the oxidation peak was splitted to one-electron coupled with one-proton reaction process for each of these two peaks. The oxidation of INH on BiO-SPEs is undergoing transfer of $2e^-/2H^+$ and subsequently hydrolyses to Isonicotinic acid. The optimal voltammetric response in Figure S4C suggested that B. R. buffer pH 2 is a suitable supporting electrolyte for determination of APAP and INH in real samples.

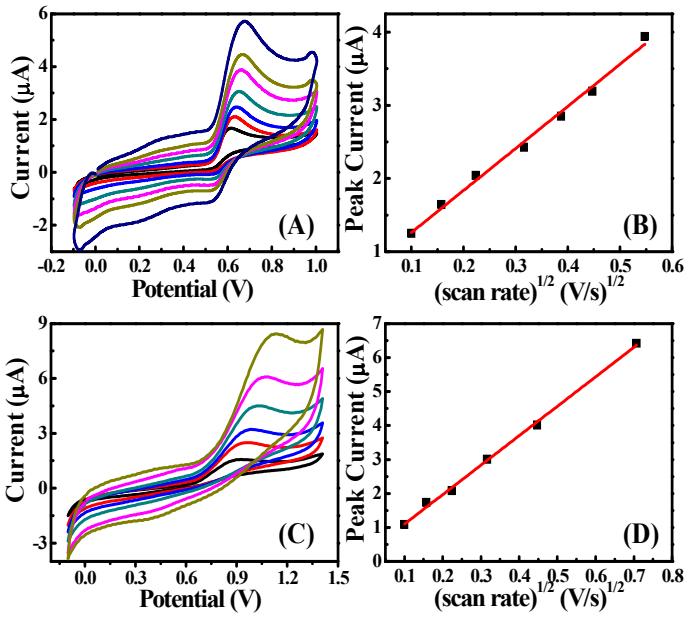

Figure 5. Effect of scan rate on cyclic voltammetric curves of 100 µM of APAP (A, and B) and 100 µM of INH (C and D) observed at BiO nanorods modified SPEs in B.R. buffer pH 2.

Next, the effect of scan rates upon the electrochemical oxidation behaviours of APAP and INH was explored in B.R. buffer pH 2.0. Figure 5 shows the cyclic voltammetric profiles of 100 µmol.L^{-1} APAP and 100 µmol.L^{-1} INH in pH 2 in different scan rate in the range of 10 –300 mVs^{-1}. No reduction peak has been observed in the cyclic voltammograms of INH. However, the intensity of APAP reduction peak becomes significant at higher scan rates. Meanwhile, there was a positive shift of peak potential with the increase of scan rates. The analysis of peak height against the square root of scan rate was found to be linear indicating a diffusional controlled processes (*For APAP;* $I_{pa}/\mu A = 5.74\ \mu A\ (Vs^{-1})^{-1/2} + 0.68\ \mu A$, $R^2 = 0.992$, *For INH;* $I_{pa}/\mu A = 8.67\ \mu A\ (Vs^{-1})^{-1/2} + 0.23\ \mu A$, $R^2 = 0.997$). Moreover, the linear relationship of log (I_{pa}) and *log υ* can be expressed as following; *For APAP: log* $I_{pa} = 0.33\ log\ \upsilon + 0.73$, *For INH: log* $I_{pa}/\mu A = 0.45\ log\ \upsilon + 0.925$. The slop values are very close to the theoretical value of 0.5, which clearly indicates a diffusion controlled electrode processes (rather than a thin layer effect). Form the above results the electro-oxidation of APAP and INH can be described as follows;

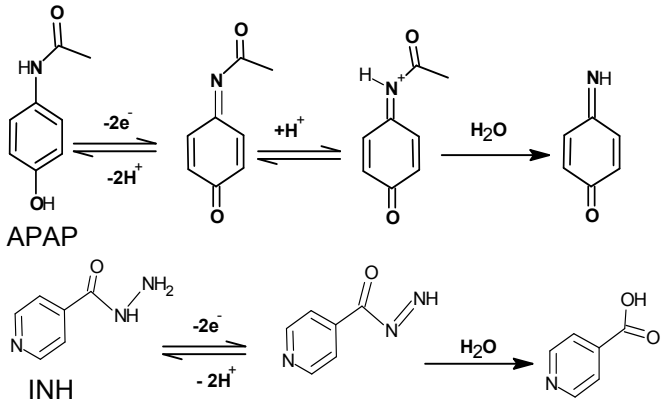

Scheme 1. Oxidation mechanisms of APAP and INH at BiO-SPEs.

Electrochemical determination of APAP and INH: Next, DPV was employed to investigate the sensitivity of BiO-SPEs in terms of linear ranges and the detection limits for the APAP and INH drugs. The DPV experiments were recorded using the following parameters; step potential 0.01 V, modulation potential 0.025 V, modulation time 0.05s, interval time 0.2s, scan rate 50 mVs^{-1}, deposition time 5s and equilibrium time 5s. Figure 6 displays the DPV responses of the electrochemical oxidation of APAP and INH using BiO-SPEs in pH 2.0 of BR buffer under the optimized working conditions. The peak height was increased with continuous additions of APAP and INH solutions. For APAP, two linear relationships were established (as shown in Figure 6B) in the range of 0.5 to 97 µmol.L^{-1} and 140 to 1250 µmol.L^{-1} as $I_p\ (\mu A) = 0.027\ \mu A \mu M^{-1} + 0.06\ \mu A\ (R^2 = 0.997)$ *and* $I_p\ (\mu A) = 0.0034\ \mu A \mu M^{-1} + 1.64\ \mu A\ (R^2 = 0.98)$, respectively. As well as, two linear segments of INH were also presented (as shown in Figure 6D) in the range of 5 to 100 µmol.L^{-1} and 144 to 1760 µmol.L^{-1} as $I_p\ (\mu A) = 0.008\ \mu A \mu M^{-1} - 0.009\ \mu A\ (R^2 = 0.99)$ and $I_p\ (\mu A) = 0.0012\ \mu A\ \mu M^{-1} + 0.49\ \mu A\ (R^2 = 0.98)$, respectively. Based on the first linear fitting equations of APAP and INH, the limits of detection were calculated to be 30 nmol.L^{-1} and 1.85 µmol.L^{-1}, respectively. The superior performance of the BiO-SPEs suggests a promising platform for the electrochemical determination of APAP and INH in real samples.

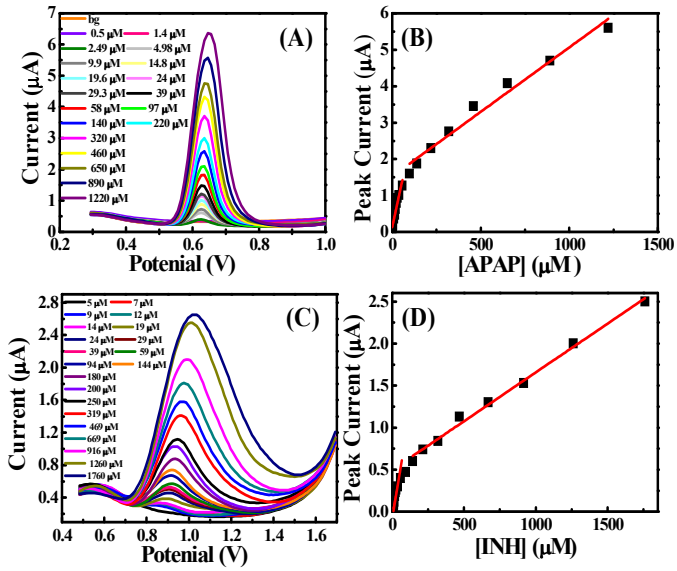

Figure 6. DPV responses from successive additions of APAP (A) and INH (C) into B.R. buffer pH 2 at BiO nanostructures modified SPEs, (B and D) Typical calibration plots corresponding to APAP and INH additions up to 1800 µM. DPV parameters: step potential 0.01 V, modulation potential 0.025 V, modulation time 0.05s, interval time 0.2s, scan rate 50 mVs^{-1}, deposition time 5s and equilibrium time 5s.

As mentioned previously, simultaneous determination of APAP and INH was studied in different pH values, and B.R. buffer pH 2.0 was selected as a suitable supporting electrolyte solution. DPV experiments for simultaneous determination of APAP and INH are carried out in pH 2.0 as represented in Figure 7. DPV of successive additions of APAP in presence of 50 µmol.L^{-1} INH revealed two well-separated and distinct oxidation peaks of APAP and INH were observed (Figure 7A). Interestingly, there was no significant change of the voltammetric response of INH with consequence additions of APAP. The calibration curve of APAP was shown in Figure 7B with the linear relationship from 10 to 210 µmol.L^{-1} with a linear equation; $I_p(\mu A) = 0.02\ \mu A\ \mu M^{-1} + 0.083\ \mu A\ (R^2 = 0.997)$. While, Figure 7C shows DPV of successive additions of INH in presence of 50 µmol.L^{-1} APAP. As can see from the voltammograms, relatively the current response of APAP does not effect by addition of INH even at high concentrations. A linear calibration curve for INH additions was presented in Figure 7D; $I_p\ (\mu A) = 0.007\ \mu A\ \mu M^{-1} + 0.937\ \mu A\ (R^2 = 0.97)$. The limits of detection of APAP and INH were calculated based on these linear fitting equations to be 37 nmol.L^{-1} and 1.61 µmol.L^{-1}, respectively. These results synergistically proved the feasibility of simultaneous determination and distinguished electrochemical sensing performance of BiO-SPEs to APAP and INH drugs as shown in Table 1.

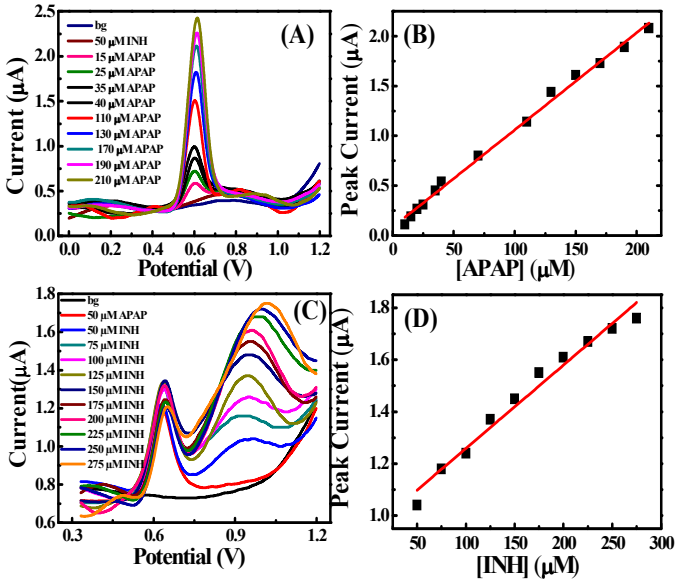

Figure 7. (A) DPV curves from successive addition of APAP in presence 50 µM INH and (B) Corresponding peak current as function of APAP concentrations. (C) DPV curves for successive addition of INH in presence 50 µM APAP and (D) Corresponding peak current as function of INH concentration. DPV parameters : step potential 0.01 V, modulation potential 0.025 V, modulation time 0.05s, interval time 0.2s, scan rate 50 mVs^{-1} , deposition time 5s and equilibrium time 5s.

Table 1. Comparisons of the proposed bismuth oxide-SPEs with previous reported electrochemical methods for APAP and INH determinations.

Electrode	Target Molecule	Linear Range (µM)	LOD (µM)	Ref.
Thionine immobilized MWCNT/CPE	APAP INH	0.1 -100 1 -100	0.05 0.8	[29]
EGR,ZnO/GCE	APAP	0.02 – 10	33	[48]
Tyrosine/GCE	INH	25-125	6.93	[49]
Fe_3O_4/PDDA/GR/GCE	APAP	0.1–100	0.037	[50]
AuNP–MWCNT/GCE	INH	0.2 – 10	0.0003	[51]
MIPRu–AuNP–MCNT/GCE	INH	0.1-110	0.08	[52]
OMC/GC	INH	0.1-370	0.084	[53]
ERGO/GCE	INH	2-70	0.17	[54]
RGO–Au/GCE	INH	10-1000	0.01	[55]
(MWCNT–chit/GCE)	INH	10-100	0.055	[56]
GR/GCE	APAP		0.032	[57]
Au and glutamic Acid /CPE	APAP	0.05-70		[58]
GCE	APAP	4-100	0.369	[59]
TiO_2–GR/GCE	APAP	1-100	0.21	[5]
BiO-SPEs	APAP INH	0.5 – 97 5 - 100	0.03 1.85	This work

Repeatability of BiO-SPEs for APAP and INH determination: Screen-printed electrode is a favourable approach in electroanalytical chemistry because it provides a low cost, single-shot disposable yet highly reproducible and reliable platform for electrochemical measurement of the target analyte. However, the sensitivity and selectivity are major challenge. Therefore, the modification of SPEs with active nanomaterials or bio-recognition events has been developed. The reproducibility of BiO-SPEs was investigated by using the same BiO-SPEs for five repetitive measurements of 50 $\mu mol.L^{-1}$ APAP and 100 $\mu mol.L^{-1}$ INH under the optimum conditions. The relative standard deviation was calculated to be 0.27 % and 0.08 % for APAP and INH respectively. Furthermore, BiO-SPEs show not only reproducible signal on the same electrode but also with separately employed SPEs. Three electrodes were examined in presence of 50 $\mu mol.L^{-1}$ APAP and 100 $\mu mol.L^{-1}$ INH under the same conditions. The relative standard deviation was calculated to be 1.7 % and 2.1 % for APAP and INH drugs, respectively. These results revealed that BiO nanorods are promising materials in electrochemical determination of APAP and INH in real samples.

Analysis of real samples: To verify the applicability of BiO-SPE sensor, the recovery experiment for determination APAP and INH in a human serum environment was performed as in section 2.4. Before DPV determination, the APAP and INH were spiked into human serum and left it for 30 minutes in fridge at 4 ^oC. Then, these spiked samples were added to 10 mL electrochemical cell containing B. R. buffer pH 2.0. The concentrations of APAP and INH were determined by standard addition protocol. The results were summarized and listed in Table 2. The recovery experiment for human serum samples demonstrated that the BiO-SPE electrochemical sensing platforms held great promise for reliable and sensitive application in the clinical analysis.

Table 2. Determination of APAP and INH added in human serum samples using DPV (each sample was measured three times n = 3).

Blood serum	Added (µM)		Detected (µM)		Recovery (%) ± SD[a]	
	APAP	INH	APAP	INH	APAP	INH
Sample 1	10	40	9.8	37.2	98 ± 1.94	93 ± 3.15
	15	60	15.3	62.4	102 ± 2.04	104 ± 4.17
Sample 2	10	40	10.2	39.2	102 ± 1.49	98 ± 2.44
	15	60	15.4	55.2	102.7 ± 1.75	92 ± 4.34

[a] *Relative standard deviation.*

Moreover, to explore the applicability of BiO-SPEs in simultaneous and sensitive determination of APAP and INH, The recovery experiments were performed in human blood, urine and saliva samples. As explained in experimental section, the APAP and INH were injected to the human fluid samples and stored at 4 ^oC in a refrigerator. After 1.0 h, the human blood was centrifuged for 5 min at 3500 rpm. The supernatant serum sample containing APAP and INH was col-

lected in a new test tube and the pH was adjusted to pH 2 by HCl. A 100 µL of treated serum samples was dropped onto BiO-SPEs cell, DPV was utilised and the standard addition method was used to determine the APAP and INH concentrations. On other hand, 300µL of urine or saliva samples was injected by APAP and INH and stored at 4 ^{o}C in refrigerator for 1.0 h. The sample solution was adjusted to pH 2 using HCl and dropped onto BiO-SPEs and DPV was utilised. Further, the APAP and INH were determined in pharmaceutical dosage. The concentrations or "recoveries" of APAP and INH were obtained. As shown in Figure S5 and Table 3, BiO-SPEs are promising candidates in determination of APAP and INH in different matrix samples.

Table 3. Recovery of APAP and INH in different real samples measured by DPV using 3-electrode BiO-SPEs configuration cell (each sample was measured three times n = 3).

ample	Added/mM		Detected/mM		Recovery (%) ± SD[a]	
	APAP	INH	APAP	INH	APAP	INH
Human blood	0.25	0.50	0.213	0.475	85 ± 4.04	95 ± 2.10
Urine samples	2.0	2.0	2.2	1.96	111 ± 3.09	98 ± 1.04
	1.0	4.0	1.09	3.96	109± 4.34	99 ± 2.50
	0.40	1.50	0.43	1.45	108 ± 3.75	97 ± 2.30
Saliva Samples	2.0	2.0	2.08	2.04	104 ± 3.2	102 ± 2.01
	1.0	3.0	1.08	3.15	108 ± 2.1	105 ± 1.02
Pharmaceutical Tablets	0.25	0.25	0.245	0.253	98 ± 2.08	101.2 ± 3.2
	0.1	0.1	0.103	0.099	103 ± 3.05	99 ± 3.6

CONCLUSIONS

A simple and one –pot hydrothermal synthesis of bismuth-rich bismuth oxide ($Bi_2O_{2.33}$) nanorods has been developed for the first time. The bismuth oxide powder was casted onto screen-printed electrode mutually facilitate the electron transfer and mass transport as well as electrocatalytic activity toward oxidation of APAP and INH drugs. The unique properties of bismuth oxide in terms of porosity, surface area and nano-scale dimension offered remarkable decrease in overvoltage and improved electrochemical response of APAP and INH drugs. Furthermore, the BiO–SPEs were applied for the determination of APAP and INH in human serum with satisfying results, indicating that BiO-SPEs can be a promising electrode material for on-site determination of APAP and INH drugs.

ASSOCIATED CONTENT

CVs of potassium Ferricyanide solution on SPE and BiO-SPE at different scan rates, CVs of APAP and INH in different pHs and relation between peak potential and pH of solution. DPV response of real sample measurements

The Supporting Information is available free of charge on the ACS Publications website.

AUTHOR INFORMATION

Corresponding Author

Email: mohamed.khairy@science.sohag.edu.eg, Tel: +(02)01092099116

Email: c.banks@mmu.ac.uk

ACKNOWLEDGMENT

The authors acknowledge funding from a British Council Institutional Link grant (No. 172726574, ID: 18435) for the support of this research.

REFERENCES

(1) Russmann, S.; Kullak-Ublick, G. A.; Grattagliano, I. *Curr Med Chem*., **2009**, *16*, 3041–3053.
(2) Friedman, S. E.; Grendell, J. H.; McQuaid, K. R. Current diagnosis & treatment in gastroenterology. New York: Lang Medical Books/McGraw-Hill., **2003**, 664–679.
(3) Darvas, F.; Guttman, A.; Dormán, G. Chemical Genomics and Proteomics, second addition, CRC Press, Taylor & Francis group, LLC, New York, **2013,** 138.
(4) Lee, W. M. *Clin Liver Dis*., **2013**, *17*, 575-586.
(5) Fan, Y.; Liu, J.-H.; Lu, H.-T.; Zhang, Q. *Colloids Surface B*, **2011**, *85*, 289–292.
(6) Prabakar, S.J.R.; Narayanan, S.S. *Talanta*, **2007**, *72*, 1818.
(7) Andersson, D.A.; Gentry, C.; Alenmyr, L.; Killander, D.; Lewis, S. E.; Andersson, A.; Bucher, B.; Galzi, J-L.; Sterner, O.; Bevan, S.; Högestätt, E. D.; Zygmunt, P. M. *Nat Commun*. **2011**, *2,* 551.
(8) Burgot, G.; Auffret, F.; Burgot, J.L. *Anal. Chim. Acta* **1997**, *343* 125.
(9) Sirajuddin, A.R.; Khaskheli, A.; Shah, M.I.; Bhanger, A., Niaz, S., Mahesar, S. *Spectrochim. Acta Part A* **2007**, *68*, 747.
(10) Ruengsitagoon, W.; Liawruangrath, S.; Townshend, A. *Talanta* **2006**, *69*, 976.
(11) Selvan, P.S.; Gopinath, R.; Saravanan, V.S.; Gopal, N.; Kumar, S.A.; Periyasamy, K. *Asian J. Chem*. **2007**, *19*, 1004-1010.
(12) Zhaoa, S.; Baib, W.; Yuana, H.; Xiaoa, D. *Anal. Chim. Acta* **2006**, *559*, 195–199.
(13) Capella-Peiro, M.E.; Bose, D.; Rubert, M.F.; Esteve-Romero J. *Chromatogr, J. B* **2006**, *839*, 95-101.
(14) Sun, D.; Zhang, H.J. *Microchim. Acta* **2007**, *158*, 131-136.
(15) Mingqi, L.; Linhai, J. Electrochim. Acta, **2007**, *52*, 3250.
(16) Kumar, S.A.; Tang, C.F.; Chen, S.M. *Talanta* **2008**, *76*, 997.
(17) Cumba, L. R.; P.Smith, J.; Zuway, K. Y.; Sutcliffe, O.B.; doCarmo, D. R.; Banks, C. E. *Anal. Methods* **2016**, *8*, 142.

(18) Byrd, C.B.; Nelson, R.; Elliott, R.C. *JAMA* **1972**, *220*, 1471–1473.
(19) Kauffman, G. B.; *J .Chem. Educ*., **1978**, *55*, 448.
(20) Tafazoli, S.; Mashregi, M.; O'Brien, P. J. *Appl. Pharmcol*., **2008***, 229*, 94–101.
(21) Epstein, M. M.; Nelson, S. D.; Slattery, J. T.; Kalhorn, T. F.; Wall, R. A.; Wright, J. M. *clin. Br. J.* **1991**, *31*, 139-142.
(22) Murphy, R.; Swartz, R.; Watkins, P.B.; *Ann Intern Med*., **1990**, *113*, 799-800.
(23) Yan, H.; Zhou, Y.; Xie, Q.; Zhang, Y.; Zhang, P.; Xiao, H.; Wang, W.; Yao, S. *Anal. Methods* **2014**, *6*, 1530-1537.
(24) Safavi, A.; Karimi, M.A.; Hormozi Nezhad, M.R.; Kamali, R.; Saghir, N. *Spectrochimica Acta Part A*, **2004**, *60*, 765–769.
(25) Wu, B.; Wang, Z.; Xue, Z.; Zhou, X.; Du, J.; Liu, X.; Lu, X. *Analyst* **2012**, *137*, 3644-3652.
(26) Liu, Y.; Fu, Z.; Wang, L. *Luminescence* **2011**, *26*, 397–402.
(27) Si, X.; Jiang, L.; Wang, X.; Ding, Y.; Luo, L. *Anal. Methods* **2015**, *7*, 793-798.
(28) Bergamini, M.F.; Santos, D. P.; Zanoni, M. V. B. *Bioelectrochem*., **2010**, *77,* 133–138.
(29) Shahrokhian, S.; Asadian, E. *Electrochimica Acta*. **2010**, *55*, 666–672.
(30) Mahmoud, B. G.; Khairy, M.; Rashwan, F. A.; Foster, C. W.; Banks, C. E. *RSC Adv*., 2016, 6, 14474–14482.
(31) Smith, J. P.; Metters, J. P.; Irving, C.; Sutcliffe, O. B.; Banks, C. E. *Analyst* **2014**, *139*, 389–400.
(32) Kolliopoulos, A.V.; Dimitrios K. Kampouris, D.K.; Banks C.E. *Anal. Chem.,* **2015***, 87,* 4269–4274.
(33) Smith, J. P; Metters, J.P.; Khreit, O.I.; Sutcliffe, O.B.; Banks, C.E. *Anal. Chem.,* **2014***, 86,* 9985–9992.
(34) Metters, J. P.; Kadara, R. O.; Banks, C. E. *Analyst* **2011**, *136*, 1067–1076.
(35) Metters, J. P.; Kadara, R. O.; Banks, C. E. *Analyst* **2013**, *138*, 2516–2521.
(36) Khairy, M.; Choudry, N. A.; Oustai, M.; Kampouris, D.K.; Kadara, R.O.; Banks, C. E. *Chem. Phys. Chem*. **2010**, *11*, 875.
(37) Khairy, M.; Kadara, R. O.; Kampouris, D. K.; Banks, C. E.; *Anal. Methods* 2010, 2, 645.
(38) Liu, L.; Jiang, J.; Jin, S.; Xiab, Z.; Tang, M. *Cryst. Eng. Comm*. **2011**, *13*, 2529–2532.
(39) Guenther, G.; Kruis, F. E.; Guillon, O. *J. Phys. Chem. C*., **2014**, *118*, 27010−27019.
(40) Liu, A.; Wei, M.; Honma, I.; Zhou H. *Anal. Chem*. **2005**, *77*, 8068 8074.
(41) Khairy, M.; El Safty, S.A. *Sens. Actuators B*., **2014**, *193*, 644–652.
(42) Khairy, M.; El-Safty, S. A.; Ismael, M.; Kawarada, H. *Appl. Cat. B: Environmental*, **2012**, *123*, 162-173.
(43) Song, J- M.; Mao, C.- J.; Niu, H.-L.; Shen, Y. -H.; Zhang, S.-Y. *Cryst. Eng. Comm*., **2010**, *12*, 3875–3881; Muruganandham, M.; Amutha, R.; Lee, G.-J.; Hsieh, S.-H.; Wu, J. J.; Sillanpaa, M. *J. Phys. Chem. C* **2012**, *116*, 12906−12915.
(44) Jiang, H.; Hu, J.; Li, C.; Gua, F.; Ma, J. *CrystEngComm*, **2010**, *12*, 1726–1729.
(45) Minami, H.; Kinoshita, K.; Tsuji, T.; Yanagimoto, H. *J. Phys. Chem. C*, **2012**, *116*, 14568–14574.
(46) Chen, R.; Ho So, M.; Che C.-M.; Sun, H. *J. Mater. Chem.*, **2005**, *15*, 4540–4545.
(47) Pei L.Z.; Wei, T.; Lin, N.; Zhang, H. J. Alloys Compd. **2016**, *663*, 677e685.
(48) Jiang, L.; Gu, S.; Ding, Y.; Jiang, F.; Zhang, Z. *Nanoscale*, **2014**, *6*, 207.
(49) Cheemalapati, S.; Devadas, B.; Chen, S.-M.; Ali, M. A.; Al-Hemaid, F. M. A. *Anal. Methods* **2014**, *6*, 6774.
(50) Lu, D. B.; Zhang, Y.; Wang, L.; Lin, S. X.; Wang, C. M.; Chen, X. F. *Talanta* **2012**, *88*, 181–186.
(51) Wu, B.; Hou, L.; Zhang, T.; Han, Y.; Kong, C. *Anal. Methods* **2015**, *7*, 9121.
(52) Wu, B.; Wang, Z.; Xue, Z.; Zhou, X.; Du, J.; Liu, X.; Lu, X. *Analyst* **2012**, *137*, 3644.
(53) Yan, X.; Bo, X.; Guo, L. *Sens. Actuators B*., **2011**, *155*, 837–842.
(54) Cheemalapati, S.; Palanisamy, S.; Chen, S.-M. *Int. J. Electrochem. Sci.*, **2013**, *8*, 3953 – 3962.
(55) Guo, Z.; Wang, Z.Y.; Wang, H. H.; Huanga G. Q., Li. M. M. *Mater. Sci. Eng. C*., **2015**, *57*, 197–204.
(56) Satyanarayana, M.; Reddy, K. K.; Gobi, K. V. *Anal. Methods* 2014, 6, 3772.
(57) Kang, X.; Wang, J.; Wu, H.; Liu, J.; Aksay, I. A.; Lin, Y. *Talanta*., 2010, 81, 754–759.
(58) Zhang, Y.; Luo, L.; Ding, Y.; Liu, X.; Qian, Z. *Microchim Acta*, **2010**, *171*, 133–138.
(59) Engin, C.; Yilmaz, S.; Saglikoglu, G.; Yagmur, S.; Sadikoglu, M. *Int. J. Electrochem. Sci*., **2015**, *10*, 1916 – 1925.

Insert Table of Contents artwork here